ADVANCED ENGINEERING MATERIALS
www.aem-journal.com

Mechanical Properties of Nanocrystalline and Amorphous Gallium Oxide Thin Films

*Anil K. Battu and Chintalapalle V. Ramana**

Nanocrystalline and amorphous Ga2O3 films (≈200 nm) with variable structural quality are produced by sputter-deposition by varying the substrate temperature ($T_s = 25$–$700\,^{\circ}C$). The effect of T_s is significant on the microstructure and mechanical behavior of Ga_2O_3 films. The variation in mechanical behavior studied by nano-indentation and nano-scratch testing reveal distinct trends, which are directly related to the structure and morphology of Ga_2O_3 films. All the Ga_2O_3 films deposited at $T_s < 500\,^{\circ}C$ are amorphous; the amorphous-to-crystalline transformation occurs at $T_s = 500\,^{\circ}C$. Ga_2O_3 films deposited at $T_s \geq 500\,^{\circ}C$ are nanocrystalline, β-phase. The corresponding mechanical characteristics, namely the hardness (H) and elastic modulus (E_r), show a strong correlation with structural characteristics. The H and E_r increases from 17 to 27 GPa and 250 to 290 GPa, respectively, with increasing T_s from 25 to 700 °C. The plasticity index, which is the ratio of H/E_n is almost constant for the Ga_2O_3 films. The strain-rate sensitivity measurements performed to determine the applicability in practical applications indicate the best performance of size controlled, nanocrystalline Ga_2O_3 films, which can be mechanically regarded as nano-composite structures. The mechanical characteristics, scratch behavior, and strain rate sensitivity indicate the role of microstructure on the mechanical performance of Ga_2O_3 films.

1. Introduction

Over the past 20 years, a great deal of research efforts have been directed toward the development of oxide semiconductor devices for practical applications in several industries.[1,2] Generally, the promising advantages of wide band gap oxides have attracted the scientific and engineering research community to utilize them in electronics, photonics, catalysis, electro-optics, integrated sensors, magneto-electronics, photovoltaics, and other energy related applications.[3–8] Very high level of tolerance to the high applied electric fields and high break-down electric field, which increase with the magnitude of energy gap, are quite attractive features of these oxides for utilization in high power and high frequency devices.[1,2,9] Among these wide band gap oxides, the scientific and technical merits and potential of gallium oxide (Ga_2O_3) have been widely recognized. Ga_2O_3, which is a stable oxide of Ga, has been identified as the promising candidate material for many technological applications in electronics, photonics, electro-optics, opto-electronics, photo-catalysis, chemical sensing, and magneto electronics.[10–17] It has been shown that Ga_2O_3 with wide band gap exhibits acceptable photocatalytic performance to decompose different pollutants or organic dyes under UV and visible-light irradiation at different phases, stoichiometries, and morphologies. Under optimized conditions, Ga_2O_3 has been shown to have a better photocatalytic performance in comparison to commercial TiO_2 particles, due to its ability to provide photogenerated charge carriers with more suitable redox potentials, leading to higher driving forces for photocatalysis.[18] Ga_2O_3 exhibits diverse structures, quite interesting material properties, and thermodynamic stability.[2,19,20] Thin films and nanostructures of Ga_2O_3 find numerous applications in high-temperature sensors, electronics, luminescent phosphors, antireflection coatings, lithium batteries, and solar cells.[14,21–24] Currently, the innovative approaches to tailor the functionality and/or promising future applications are driving the scientific and research thrust in single-phase Ga_2O_3 as well as Ga_2O_3-based multi-component architectures or hybrid materials with nanostructured morphologies. However, control over the phase, structure, and mechanical and electronic properties is the key for their integration into practical device applications.

Gallium oxide exhibits polymorphism. The α, β, γ, δ, and ε phases of Ga_2O_3 are widely known.[16,18,25–27] Among these polymorphs, monoclinic β-Ga_2O_3 is thermally stable with a band gap of ≈5 eV and high breakdown field 8 MV cm^{-1}.[28] β-Ga_2O_3 exhibits n-type conductivity, which is related to donor centers involving oxygen vacancies and/or impurities. The high thermal stability of β-Ga_2O_3 (melting point ≈1900 °C) is quite useful in the design and development of high-temperature chemical sensors, which can be readily used in automotive industry and power plants.[2] Furthermore, the high-temperature stability coupled with deep ultraviolet transparency makes Ga_2O_3 based materials as the potential candidates for chemical sensors in extreme environments and transparent electrodes in UV optoelectronics, photonics, and thin-film transistors.[29–31] However, in all these applications, fundamental understanding of the structure, thermodynamic conditions, and mechanical characteristics is the key to achieving enhanced device performance.

Prof. C. V. Ramana, A. K. Battu
Department of Mechanical Engineering
University of Texas at El Paso
El Paso, Texas 79968, USA
E-mail: rvchintalapalle@utep.edu

DOI: 10.1002/adem.201701033

Recent developments in surface coating technology, particularly in the production of nanostructured films, have revealed exciting possibilities to control hardness and elastic modulus with some degree of independence, thereby producing wear-resistant surfaces with combinations of properties which were previously unobtainable.[32] Current scientific thrust to produce the so-called "nanocomposite" coatings is directed primarily toward the design and development of super-hard or ultrahard wear resistant materials.[33,34] The performance of these nanocrystalline materials is closely connected to their microstructure, phase, and also depends on the mechanical characteristics to improve the desired properties for a given technological application.[35,36] In fact, the designing of materials must combine excellent properties, or comparable to those of the currently used materials, with excellent hardness and elastic modulus, good adhesion, toughness, durability on Si with low interface stresses, which are quite essential for their utilization in extreme environment applications, especially in automotive and coal-based power plant industries.[37,38] Under such conditions, it becomes critical to understand how the structural modifications (if any) affect the properties, most importantly the mechanical characteristics which determine their survivability. Therefore, a fundamental understanding of the mechanical characteristics of Ga_2O_3 nanostructures is essential for utilizing them in energy related applications, such as absorber layers in concentrated solar power plants and integrated sensors in oxy-combustion as encountered in engine technologies and coal-based power plants. Under the specific conditions, the materials' ability and survivability to sustain sudden impact loads or temperature fluctuations is of major concern.[39] Thus, a fundamental knowledge and a deeper understanding of the mechanical properties and how these characteristics depend on the microstructure is quite important to effectively utilize Ga_2O_3 under the presence of extreme environment and/or energy related applications. However, unfortunately, while Ga_2O_3 proven to be good candidate for such applications, especially involving exhaust systems of engines and energy storage and conversion technologies, the efforts to understand the mechanical stability of Ga_2O_3-based nanomaterials is meager. On the other hand, in the context of evolving new hybrid materials based on Ga_2O_3 for energy related applications as well as new technological applications of Ga_2O_3, a fundamental knowledge of mechanical properties of intrinsic Ga_2O_3 films is quite important. Thus, the primary objective of this work is to fill this knowledge gap by establishing a structure-mechanical property relationship in nanocrystalline and amorphous Ga_2O_3 films. Thus, we have focused our efforts and employed a range of deposition conditions to produce Ga_2O_3 films with variable microstructure. Recent studies suggest that the mechanical properties of Ga_2O_3 in perfect 2D form which are obtained from liquid metals can provide extraordinary opportunities for enhancing such characteristics.[40,41] Furthermore, much of the recent research on nanocomposite super-hard coatings has been focused purely on hardness; however, lately, it has been realized that the toughness and plasticity index are important in many of the aforementioned technological applications. Therefore, we performed a comprehensive study in order to understand the interplay between the structure, mechanical properties, and performance of Ga_2O_3 films which leads to obtain strong Ga_2O_3 sheets in future.

2. Experimental Section

2.1. Fabrication

The Ga_2O_3 films were deposited onto silicon (Si) (100) wafers by radio-frequency sputtering. All the substrates were thoroughly cleaned and dried with nitrogen before introducing them into the vacuum chamber, which was then evacuated to a base pressure of $\approx 10^{-6}$ Torr. The deposition was made by sputtering of Ga_2O_3 ceramic target. Ga_2O_3 ceramic target (Plasmaterials, Inc.) of 2 in. diameter and 99.999% purity was employed for all the depositions. The target was placed on a 2 in. sputter gun, which were placed at a distance of 7 cm from the substrate. A sputtering power of 40 W was initially applied to each target while introducing high-purity argon (Ar) into the chamber to ignite the plasma. Once the plasma was ignited the power for each target was increased to their respective sputtering power for reactive deposition. The flow of Ar and oxygen (O_2) were controlled using an MKS mass flow meters. Before each deposition, the target were pre-sputtered for 15 min with a closed shutter above the gun. The deposition was carried out to produce Ga-oxide films with a constant thickness of 200 ($\pm$10) nm. The deposition time was then kept constant for sputtering of the gallium oxide target in order to produce the Ga_2O_3 films. Deposition of Ga_2O_3 samples was carried by keeping Ga_2O_3 sputtering power constant at 100 W. The samples were deposited at different substrate temperatures (T_s) varying in the range from room temperature ($RT = 25\,^{\circ}C$) to 700 °C. Substrate rotation is maintained during the entire deposition time to ensure uniform coverage on the substrate surface.

2.2. Grazing Incidence X-Ray Diffraction (GIXRD)

The gallium oxide films were characterized by performing crystal structure, elemental composition, surface morphology, and mechanical property measurements. The crystal structure analysis was performed by using Grazing Incidence X-ray Diffraction (GIXRD) equipment (Bruker D8 advance, Cu-*Ka* radiation, and $\lambda = 1.54$ Å) at room temperature. The grazing incident angle was fixed to 1° for the incoming X-ray beam, so that used to study only surfaces and layers for the thin films. The detector scan varies from 10° to 67° at a scan speed of 0.5 s step^{-1}.

2.3. Scanning Electron Microscopy (SEM)

The surface morphology analysis was performed using high performance and ultra-high-resolution scanning electron microscope (Hitachi S-4800). Secondary electron topographical imaging was performed using the conductive silver paint at the ends of the samples which are attached to sample holder by carbon tape to avoid the charging problems.

2.4. Mechanical Properties

The deposited films were analyzed to determine their mechanical properties; hardness (H) and reduced elastic modulus (E_r) were

obtained by nanoindentation tests (Hysitron T1750 Tribo nanoindenter). Nanoindentation measurements were made employing a triangular pyramid Berkovich diamond indenter with a normal angle of 65.3° between the tip axis and the faces of the triangular pyramid and the effective size of the apex was about 100 nm. A commonly accepted rule suggests that the substrate measurements can be obtained if the indentation depth is kept less than 10% of the film thickness. At such small indentation loads, the indents on the films can be microscopic to submicroscopic in size. So, measuring these small indents is very difficult and not accurate. Therefore, the most common method so far has been to gauge the size of the indentation from the loading and unloading curves generated during the test performance. The deformation during loading is assumed to be both elastic and plastic tendency, whereas, during unloading, it is assumed that only elastic displacements are recovered which is the elastic nature of the unloading curve that facilitates analysis. Therefore, the standard procedure was employed to derive the mechanical properties with the help of loading and unloading curves.[42,43] The method developed by Oliver and Pharr was employed to calculate the mechanical characteristics (H and E_r). Using this approach, E_r can be calculated by finding the stiffness (S) of the film from the slope of the unloading curve; the relation between E_r and S can be described using:

$$E_r = \frac{\sqrt{\pi}}{2}\frac{S}{\sqrt{A}} \tag{1}$$

where A is defined as the area of contact at peak load. To find the hardness values, the same value for the area of contact is used along with the maximum load (P_{max}) in:

$$H = \frac{P_{max}}{A} \tag{2}$$

Load controlled indentation tests were performed initially on each sample to determine the maximum depth that would not be more than 10% of the total film thickness to minimize the substrate effect. Seventeen indents of selected 350 μN load were performed at 0.1 s^{-1} strain rate, and the average of H and E_r values were calculated on each sample.

Film or coating adhesion is one of the paramount characteristics that is related the coating quality and life.[44–46] The deposited film adhesion was analyzed by nano-scratch test (Hysitron T1750 Tribo nanoindenter). This test was performed at room temperature under the load increments from 0 to 8000 μN. The same standard triangular pyramid Berkovich diamond indenter tip has been used. The length of the scratch was 16 μm, and the scratch speed was 0.18 μ s^{-1}.

3. Results and Discussion

3.1. Crystal Structure

The GIXRD patterns of Ga_2O_3 films are shown in **Figure 1** as a function of T_s. The very first characteristic nature that can be noted is the clear variation in the diffraction patterns with increasing T_s. The Ga_2O_3 films deposited at RT exhibit diffuse pattern, which did not show any diffraction peaks, indicating the amorphous nature

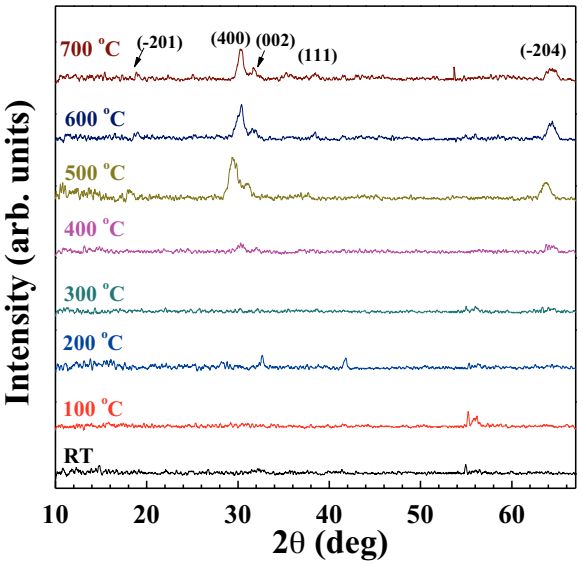

Figure 1. X-ray diffraction patterns of Ga_2O_3 films. The effect of T_s on the evolution of patterns can be seen. The appearance of diffraction peaks and their assignment suggest that the samples deposited at $T_s \geq 500$ °C are crystalline and stabilized in β-phase of Ga_2O_3.

of the films. The trend continues with increase in T_s from RT to 500 °C, at which point the presence of diffraction peaks began to appear. The peaks evolution in the XRD pattern at $T_s = 500$ °C indicates the film crystallization at this temperature. The XRD patterns of Ga_2O_3 films deposited at $T_s = 500$–700 °C corresponds to monoclinic β-phase (space group C2 m^{-1}) with identified peaks ($\bar{2}01$), (400), (002), and ($\bar{2}04$) at 2θ values of 18.95, 30.05, 31.74, and 64.17, respectively, according to of JCPDS (00-043-1012).[24] It can be noted that the (400) peak at $2\theta = 30.05°$ exhibits the dominance in intensity for Ga_2O_3 films. The (400) peak evolution with increasing T_s is evident; intensity of this peak increases while the peak width is reduced. These observations clearly indicate that the T_s strongly influences the growth behavior and, hence, the structure of Ga_2O_3 films. The amorphous nature of the set of Ga_2O_3 films deposited at $T_s < 500$ °C can be attributed to the lack of sufficient thermal energy to promote structural order. If T_s is low such that the period of the atomic jump process of adatoms on the substrate surface is very large, the condensed species may stay stuck to the regions where they are landing, thus leading to an amorphous Ga_2O_3 film. The adatom mobility on the surface increases with increasing T_s. The onset of diffraction peaks in XRD clearly indicate that 500 °C is the critical temperature to promote the growth of nanocrystalline Ga_2O_3 films. For the given set of experimental conditions, a temperature of 500 °C is, therefore, favorable to provide sufficient energy for Ga_2O_3 film crystallization. These results agree with our previous findings, although film thickness is quite high in this work compared to previous studies.[24]

3.2. Surface Morphology

The scanning electron microscopy (SEM) images of Ga_2O_3 films are shown in **Figure 2**. The amorphous nature is clear in the SEM

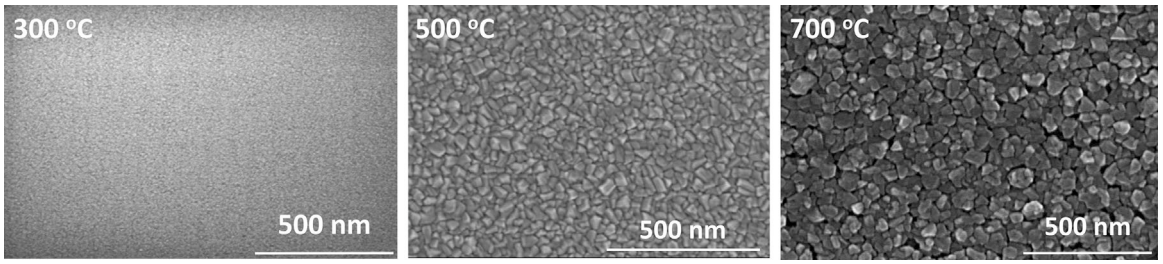

Figure 2. SEM images of Ga_2O_3 thin films as a function of T_s.

images of Ga_2O_3 films deposited at 300 °C. The images obtained are similar for Ga_2O_3 films deposited at T_s = RT–400 °C. A fine microstructure and uniform distribution of dense particles can be seen in Ga_2O_3 films grown at T_s = 500 °C. The dense morphology seen at 500 °C is more or less similar until T_s reaches 700 °C, where the particle size increases further. However, it is evident that Ga_2O_3 films deposited at 700 °C exhibit some porous structure although the average size generally increases with T_s. It should be pointed that this trend is general for oxide films and, earlier, the surface morphology variation and other properties improvement were observed for different oxides.[47–50] The average grain size increases from 15 to 35 (±2) nm with increasing T_s.

3.3. Mechanical Properties

3.3.1. Indentation Load (L)—Penetration Depth (d) Characteristics

The data of peak indentation load (L)—indentation depth (d) of the Ga_2O_3 films are shown in **Figure 3**a. Unfortunately, for thin films, the underlying substrate properties strongly influence the indentation response, and it is difficult to obtain the intrinsic properties of nanocrystalline films.[37,51] However, nano-indentation measurements are well known, reliable and provides a simple and quick method for obtaining information about the mechanical properties of thin films.[37] The reproducibility is good, but, when the ratio of indentation depth to the film thickness (d/t) exceeds a critical value, then the measured mechanical properties are going to be influenced by the substrate material and it is no longer characteristics of the coating.[43,52,53] Therefore, one needs to identify the penetration depth by monitoring the phenomena with respect to indentation load. The critical d/t ratio ≈10% is preferred. The results (Figure 3a) indicate that all the Ga_2O_3 films exhibit the same type of response to indentation load, that is, an increase in the indentation depth with respect to the increasing load. The load was varied from 100 to 2000 μN. At the initial load, that is, at 100 μN, the obtained depth was ≈8 to 9 nm for all the Ga_2O_3 films. At 350 μN load, all the Ga_2O_3 films reach the depths ≈19–21 nm which is 10% of the total thickness. Beyond this load (10% of the total thickness), the variation in penetration depth can be noted. The penetration depth increases with the increasing indentation load. The variation is ≈36 nm for a variation in T_s from RT to 700 °C while the load is constant at 2000 μN. The Ga_2O_3 film deposited at RT had a higher penetration depth, which is ≈95 ± 2 nm. The data obtained (Figure 3a) indicate that the penetration depth decreases with increase in T_s. This is due to the fact that the measured indenter penetration will be greater in the case of less dense packed or loosely packed films.[53–55] The penetration depth for Ga_2O_3 films deposited at 500–700 °C is almost the same with negligible difference of ±2 nm. The penetration depth variation is directly related to structural evolution of Ga_2O_3 films as a function of T_s. As revealed by the XRD and SEM analyses, Ga_2O_3 films deposited at T_s = RT–400 °C are fully amorphous while those deposited at T_s = 500–

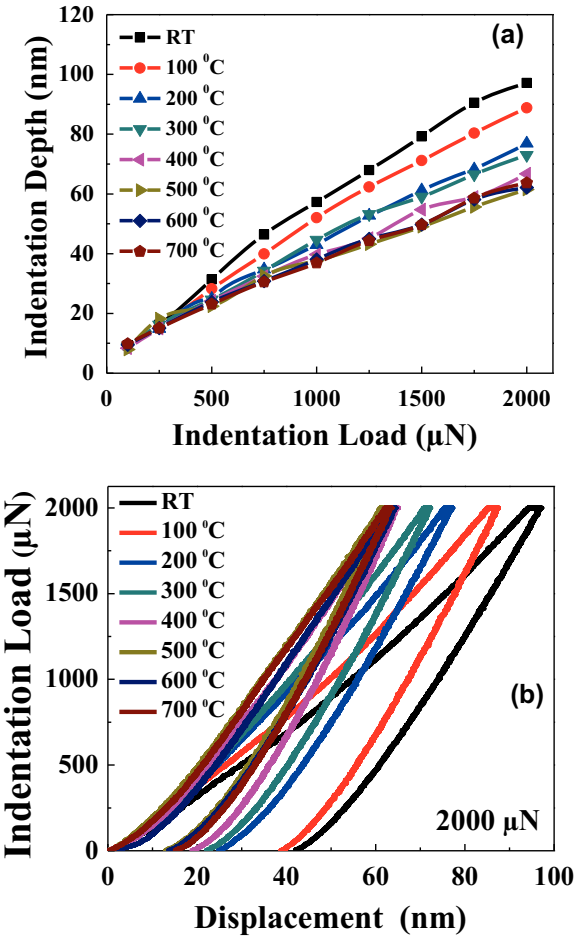

Figure 3. a) Effect of indentation load on the Ga_2O_3 films in terms of indentation depth b) Load–displacement curves of Ga_2O_3 films obtained at 2000 μN indentation load.

700 °C are nanocrystalline. Therefore, for amorphous Ga_2O_3 films, the surface is no longer stiffer to resist the penetration of indentation and, hence, the depth is greater. It should also be noted that the fully crystalline films with an excellent packing of atoms are expected to be stiffer and stronger than the films with the less dense packing of atoms. Therefore, the nanocrystalline Ga_2O_3 films deposited at $T_s = 500$–700 °C oppose to indentation resulting in the decrease of penetration depth.

The loading and unloading curves are shown in Figure 3b, where a typical load vs. displacement curves are shown. The data shown are obtained at a constant load of 2000 μN. Three important quantities can be measured from the load vs. displacement curves: the maximum load (P_{max}), maximum displacement (h_{max}), and elastic unloading stiffness (S), that is, the slope of the upper portion of the unloading curve during the initial stage of unloading. The accuracy of the H and E_r values were dependent on how well these parameters can be measured experimentally. Another important consideration was the final depth (h_f), the indentation depth of penetration after the indenter is fully unloaded.[43] The load versus displacement curves are different for Ga_2O_3 films deposited under variable T_s. Notably, the slope varies with T_s. Similar to indentation load versus penetration depth characteristics, the slope variation can be attributed to the initial amorphous nature and then amorphous to crystalline transformation of the Ga_2O_3 films with increasing T_s. However, all the nanocrystalline Ga_2O_3 films deposited in the range of 500–700 °C exhibit the loading and unloading curves with negligible differences in the slope and penetration depth.

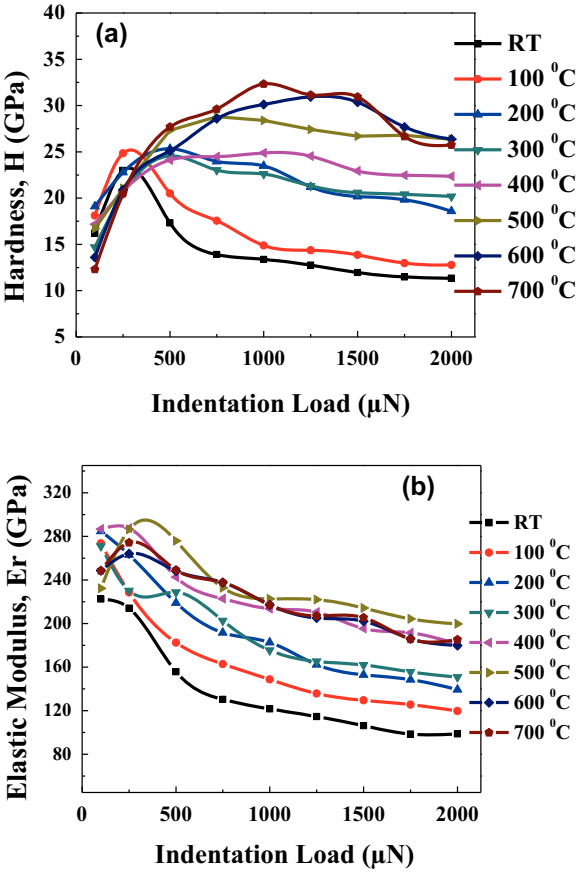

Figure 4. a) Effect of indentation load on H; b) Effect of indentation load on E_r.

3.3.2. Effect of Indentation Load (L) on Hardness (H) and Reduced Elastic Modulus (E_r)

The hardness variation of Ga_2O_3 films as a function of indentation peak load is presented in **Figure 4**a. It can be noted that there is a remarkable difference in H values of Ga_2O_3 films deposited at various T_s. For thin films, the measured hardness varies continuously with the indentation load, penetration depth, film thickness, and the substrate hardness. In the present work, the film thickness and hardness of the substrate were kept constant. Therefore, the variables are indentation load and penetration depth. Theoretically, H values depend on the (L) and d.[33,35,56,57] In the present case, the data as well as comparison indicates that the phenomena is dependent on the crystallinity of the Ga_2O_3 films. It is evident that the H values increase with increasing T_s. This is mainly due to the improved crystalline nature of Ga_2O_3 films with T_s increase, as evidenced from XRD and SEM studies. Note that the hardness is related to the bonding between the atoms and to the ability of the bonds to withstand deformation.[54] The data follows the similar trend for Ga_2O_3 films deposited at $T_s = 25$–100 °C, then H values increase slightly for Ga_2O_3 films deposited at $T_s = 200$–400 °C. Therefore, these films have similar trend and there was noticeable difference. Finally, for $T_s = 500$–700 °C, the data shows similar trend with negligible difference between the values. This negligible difference is mainly due to the grain size refinement. For these films, the hardness increases until the critical load 350 μN, at which point decreases slightly and remain constant with minimum variations. This phenomenon is mainly due to the substrate effects. In practice, in indentation experiments, penetration depth has to be maximum 10% of the total film thickness to avoid the substrate effects. Thus, both the L-d and H-L relationships are in corroboration with the observed differences in terms of structural changes of Ga_2O_3 films. The E_r variation with load in Ga_2O_3 films is shown in Figure 4b, where similar behavior is also noted in E_r data. The E_r values gradually decrease with increasing load. Also, the E_r value increases with increasing T_s. Thus, the decreasing E_r is due to structural transformation; E_r values of an amorphous material is usually lower than its crystalline counterpart because of less dense packing.[39,53]

3.3.3. H and E_r at Critical Load

To obtain the reasonable and reliable H and E_r values, the penetration depth where substrate induced effects can be safely neglected is important. The evaluation of loading and unloading curves for the Ga_2O_3 films at 350 μN, is shown in Figure 4. At 350 μN indentation load, there was an optimum displacement between the loading and unloading curves. The obtained penetration depth was ≈20 nm, which is almost 10% of the total thickness. By considering the above reasons, as well as

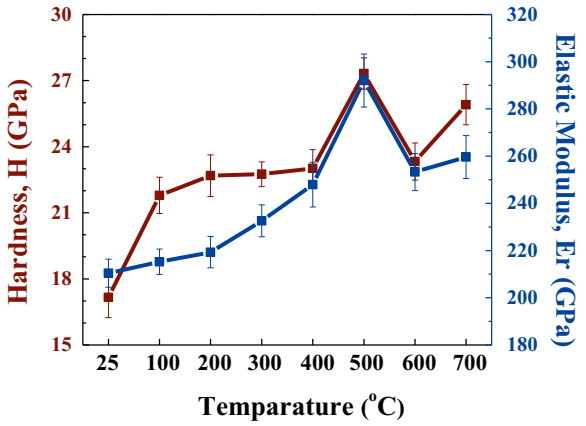

Figure 5. Hardness and elastic modulus of Ga_2O_3 films.

discussed in previous sections, we can conclude that the optimum load was 350 μN, where we can get the accurate H and E_r results. The mechanical properties of the Ga_2O_3 films deposited at 500 °C is investigated first to establish the baseline properties. This is also for the other reason that, according to XRD and SEM analyses, the realization of nanocrystalline, β-Ga_2O_3 films occurs at $T_s = 500$ °C. The H and E_r data of Ga_2O_3 films are shown in **Figure 5**. It is evident that the T_s and structural evolution significantly influences the mechanical characteristics of Ga_2O_3 films. The influence of the grain size on mechanical properties (H and E_r) is complex since the grain boundaries may either act as obstacles to dislocation slip (strengthening effect) or provide a positive contribution to the deformation of the material (softening effect).[34,58] As a result, the H values were gradually increased from 17 to 27 GPa for the Ga_2O_3 films with increasing T_s from RT to 500 °C and then remain more or less constant with further increase in T_s to 700 °C. However, the hardness of Ga_2O_3 films deposited at 700 °C slightly decreases compared to that obtained for the film deposited at 500 °C. Similarly, the E_r values also increase from ≈210 to 290 GPa. The H and E_r characteristics follow almost the similar trend (Figure 5). The observed variation and differences in the mechanical characteristics of Ga_2O_3 films can be explained as follows. Nanocrystalline materials, due to their nano sized grains and high density of interfaces show high strength and hardness, and many other interesting properties.[54] Therefore, the higher values of H and E_r observed are, undoubtedly, due to the texturing and interface microstructure of the nanocrystalline, granular Ga_2O_3 films. These parameters (E_r and H) are intrinsic mechanical property of a material dominated by the strength and chemical bonds between constituent atoms.[57,59,60] It is well known that the improvement in the strength of materials is due to its grain refinement. The role of grain boundaries is enhanced significantly with the reduction in grain size.[34,59,61] Thus, the E_r value of an amorphous material is usually lower than its crystalline counterpart because of less dense packing. Therefore, we believe and conclude that the observed changes in mechanical properties are mainly due to the microstructure changes in Ga_2O_3 films.

3.3.4. Significance of H/E_r and H^3/E_r^2

In recent years, just hardness is considered as the primary requirement for wear resistance. In addition to H, elasticity and toughness are also regarded as important factors.[32] Therefore, combined analysis and consideration of H/E_r and H^3/E_r^2 along with H and E_r has been proposed as realistic means to derive a better understanding of the mechanical behavior of nano-materials, especially nano-composite thin films and coatings.[62] From the measured values of H and E_r, H/E_r, and H^3/E_r^2 can be calculated. The H/E_r and H^3/E_r^2 data of Ga_2O_3 films is presented in **Figure 6**. The ratio between H and E_r is referred as plasticity index (sometimes it is also indicated as coating durability),[32,33,37,63] which is widely accepted as a valuable measurement for determining the limit of elastic behavior of the thin films. This ratio is important to avoid wear. The term H^3/E_r^2

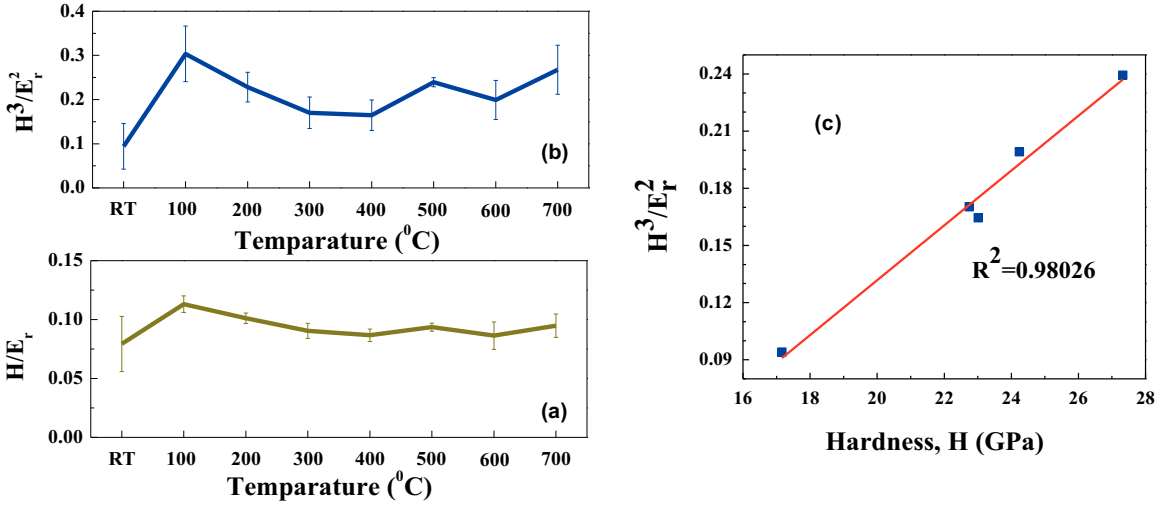

Figure 6. The effect of T_s on: a) H/E_r and b) H^3/E_r^2values. c) Linear relationship between H^3/E_r^2 and H as noted in Ga_2O_3 films.

should be a reliable indicator of a coating's resistance to plastic deformation and referred as toughness.[43] In this case, the two parameters (H/E_r and H^3/E_r^2) values and their trends will be helpful for the clear understanding the intrinsic Ga_2O_3 films mechanical behavior, especially for their integration in high-temperature sensors to be operated under extreme environments.[64] The data obtained for Ga_2O_3 films (Figure 6a) indicate that most of the films exhibit $H/E_r \leq 0.1$. Note that the Ga_2O_3 films deposited are ceramics; therefore, H/E_r ratio is expected to be less than 0.1.[52] The H/E_r ratio for the nano-crystalline Ga_2O_3 films is 0.085 ± 0.05 and almost constant. The H^3/E_r^2 data for Ga_2O_3 films are presented in Figure 6b. The H^3/E_r^2 data exhibits the similar trend as noted for H/E_r. The values are in the range of ≈0.1–0.3 GPa. The H^3/E_r^2 values were gradually increased from 0.17 to 0.24 ± 1 GPa for the crystalline Ga_2O_3 films. This is due to the variation in the grain size of these films, as explained in the previous section. Ga_2O_3 films deposited at 500 °C exhibit the highest value of H^3/E_r^2 which is $\approx 0.23 \pm 0.01$. The H^3/E_r^2 ratio is the indication of the coating resistance to plastic deformation. Therefore, higher the ratio higher the resistance to deformation.[32,37] Therefore, the H/E_r and H^3/E_r^2 indicate that Ga_2O_3 films deposited at 500 °C with a characteristic nano-crystalline and dense morphology exhibits the highest deformation resistance or toughness.

We believe that the superior mechanical characteristics of nanocrystalline Ga_2O_3 films is derived from the interconnected network of densely packed, smaller crystallites. Thus, a simple model can be formulated to explain the observed functional relationship between the mechanical characteristics (H and E_r) and structure in nanocrystalline Ga_2O_3 films. Evident from the results, the H, E_r, H/E_r, and H^3/E_r^2 depend on the structural quality and grain size. XRD and SEM results evidenced that Ga_2O_3 films deposited at RT are completely amorphous. In fact, all the films deposited at $T_s < 500$ °C are amorphous. It is, therefore, reasonable to attribute the observed low mechanical quality or lower values of H, E_r, H/E_r, and H^3/E_r^2 to a very low packing density in the Ga_2O_3 films. These films, which are characterized by a structural disorder may be causing a decrease in mechanical characteristics. However, the initial improvement or increase in H, E_r, H/E_r, and H^3/E_r^2 values when Ga_2O_3 films deposited within range of 300–400 °C is due to a slight improvement in the structure, but still mostly the amorphous structure is dominating. However, the structural transformation from amorphous-crystalline Ga_2O_3, as noted in XRD and SEM measurements, enhances the mechanical characteristics. Therefore, we believe that improved structural order results in the formation of a dense network of nanocrystals leading to an enhancement in the packing density. This characteristic change in structure results in the observed enhancement in H, E_r, H/E_r, and H^3/E_r^2. Furthermore, in nanocrystalline Ga_2O_3 films, the nanostructure is characterized by a dense, randomly oriented nanocrystals.[62] Musil et al. have defined the parameter (H^3/E_r^2) as the resistance to plastic deformation and demonstrated a general, linear relationship between H^3/E_r^2 and H for many coatings for mechanical and tribology applications.[65,66] Furthermore, using nano-indentation and nano scratch testing, Beake et al.[35] have also demonstrated such linear relationship in TiN/Si_3N_4 composites. Therefore, an attempt has been made in this work to examine the H^3/E_r^2 verses H relationship. The variation of H^3/E_r^2 with H for the Ga_2O_3 films is shown in Figure 6c, where it can be seen that the data fits approximately to a linear relationship. Perhaps, the nanocrystalline Ga_2O_3 films may be equivalent of a composite structure by virtue of nanocrystallites embedded in slightly porous structure.

3.3.5. Strain-Rate Experiments at Specific Indentation Load

Further examination of the mechanical characteristics is evaluated by indentation strain rate also called as equivalent strain rate. Mayo and Nix[67] developed a nanoindentation method for the determination of strain rate sensitivity (SRS) on a submicron level by controlling the loading rate.[67,68] The indentation strain rate was determined from the depth–time data for a given range of indentation depth. According to Mayo and Nix, the indentation strain rate can be derived from the concept of true strain. Approximating the specimen length by the indentation depth and assuming the hardness to be independent from the indentation depth, this can be estimated as:[67,69–71]

$$m_{\text{nanoindentation}} = \frac{d(\ln H)}{d(\ln \varepsilon')} \tag{5}$$

where m is the SRS exponent, which describes the SRS behavior of the material assuming a constant microstructure.

$$\varepsilon' = \frac{1\dot{P}}{2p} \tag{6}$$

where, the loading rate $(\dot{P})$ and applied maximum load (P), in other words ratio of the indenter displacement velocity to the plastic depth.

Loading rates and equivalent strain rates are directly proportional to each other, as can be seen from equation. (above equation). The hardness variation with equivalent strain rate for Ga_2O_3 films is shown in **Figure 7**. To evaluate the strain rate

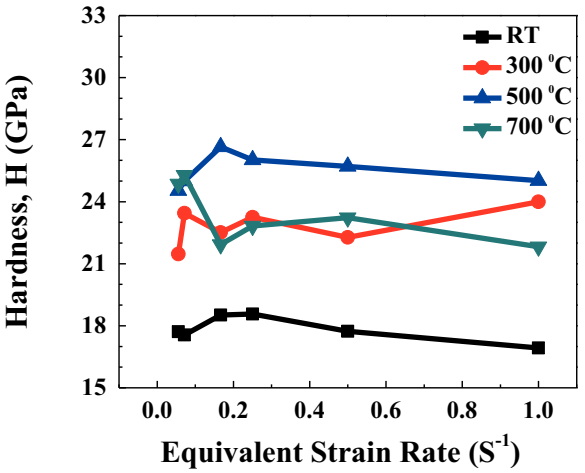

Figure 7. Variation of hardness with equivalent strain rates at constant load of 350 μN.

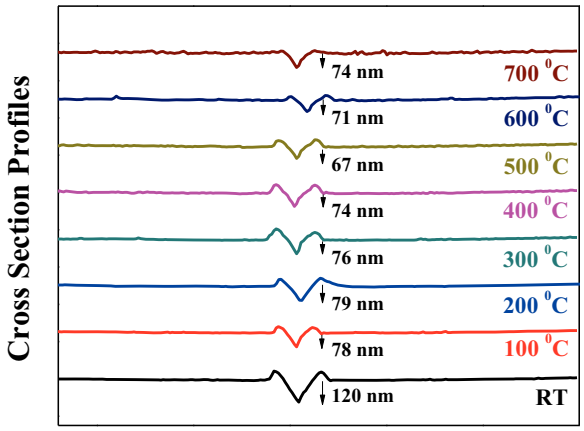

Figure 8. Scratch testing profiles of Ga_2O_3 thin films. Depth profiles for Ga_2O_3 thin films deposited at various T_s are shown. It is evident that the depth is higher in amorphous Ga_2O_3 films.

dependence of the hardness, seven different indentation strain rates (0.05, 0.07, 0.10, 0.16, 0.25, 0.50, and 1.00 s^{-1}) were applied during the nanoindentation. The average H values measured at different strain rates were performed at specific load conditions, that is, 350 μN. The trend clearly shows a distinct and experimentally detectable effect of indentation strain rates. For Ga_2O_3 films deposited at RT, the H values are continuously decrease due to the amorphous nature. However, the nanocrystalline Ga_2O_3 films showed negligible change. The strain rate sensitivity (m) is the materials resistance to prevent necking during the deformation of a material.[72,73] The measured m values were 0.017, 0.013, 0.011, 0.013 for RT, 100, 300, 500, and 700 °C, respectively. It can be observed clearly that the substrate temperature and, hence, the microstructure significantly influences the strain rete sensitivity of the Ga_2O_3 films.

3.3.6. Adhesion and Interfacial Bonding—Scratch Testing

Scratch resistance is one of the most critical parameters required for thin films coatings, such as automotive topcoats, floor coatings, and optical components.[56,74,75] Because most of the coatings encounter a wide range of mechanical stresses during their working lifetime, scratch test is one of the most prominent and widely accepted methods to evaluate the adhesion strength between the thin, hard coatings and substrates.[76,77] The depth profiles and scratch test results of Ga_2O_3 films are presented in **Figure 8 and 9**, respectively. The data reveal that the Ga_2O_3 films deposited at 500 °C exhibit the best interfacial bonding interms of depth profile, that is, 67 nm after the performance of scratch test (Figure 8). The scratch test was performed in such a way that, when the cohesive failure occurs, the area around the scratch deforms while the rest of the film remains undamaged.[33,78] It is important to recognize that the nanocrystalline Ga_2O_3 films do not exhibit any delamination other than pile up deformation. The depth (Figure 8) profiles show the cross-section of the films at the maximum applied force along the scratch. The negative scratch depth means that the indenter is located above the initial sample surface, and positive depth indicates the indenter is moved below the initial surface. The nano-scratch was performed in ramping mode, where the normal force is increasing along with the scratch X-direction. The lateral force applied on the tip by deforming material could also be used to determine plastic properties of the films. However, it was determined that a cross-section profile of the scratch when 8000 μN force is applied better demonstrate the deformation mechanisms. Evidently, the depth profile cross-sections obtained at the maximum 8000 μN force exhibits that the scratch depth was continuously decreasing with increasing crystallinity. This behavior matches with the H behavior shown in Figure 4. The depth profiles were almost constant for the films with minimal variation, that is, all the

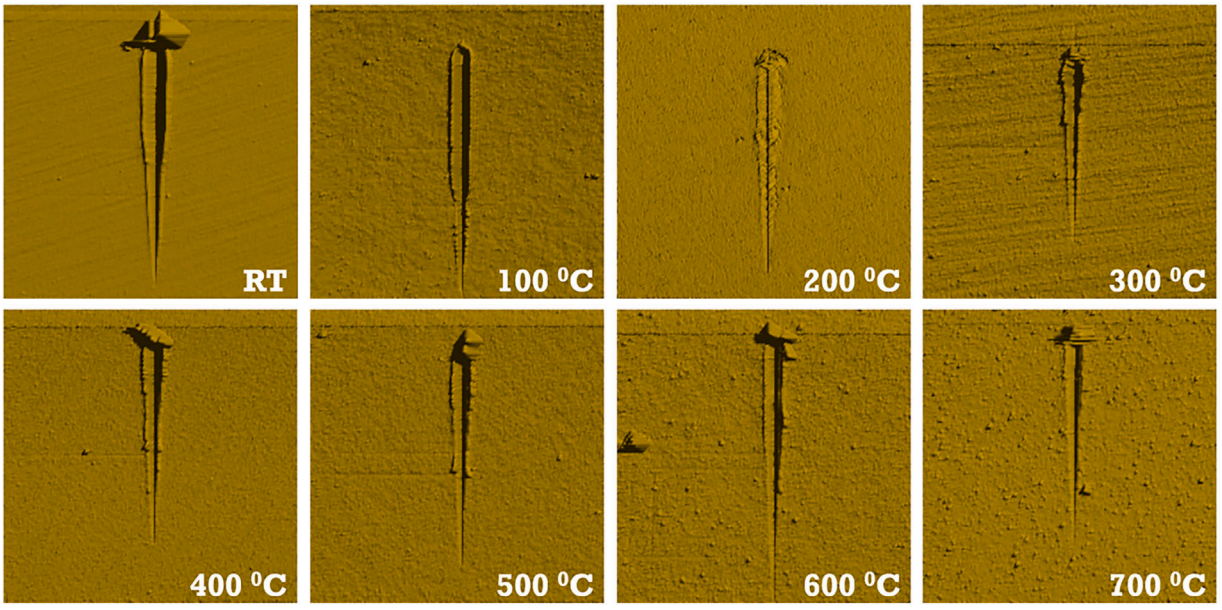

Figure 9. Scratch testing data of Ga_2O_3 films, surface images after scratch test are shown.

films lied between 67 to 74 nm which is following the H^3/E_r^2 trend. As discussed, the H^3/E_r^2 ratio is proportional to the coating resistance to plastic deformation, which indicates higher the ratio higher the deformation resistance. Also, it should be noted that nano-scratch (**Figure 9**) tests showed material pile-up, but no evidence of channel cracking or delamination of the films was observed.

4. Summary and Conclusions

The Ga_2O_3 nanocrystalline thin films were sputter deposited onto Si (100) by varying the substrate temperatures from RT to 700 °C. The effect of T_s on the crystal structure, surface morphology and mechanical characteristics of Ga_2O_3 films is investigated. The results indicate that Ga_2O_3 films deposited at T_s = RT–400 °C were amorphous and those deposited at $T_s \geq 500$ °C were nanocrystalline with a stable β-phase. The nanocrystalline Ga_2O_3 films exhibit excellent mechanical properties. The hardness increases from 17 to 27 GPa and elastic modulus from 250 to 290 GPa with increasing T_s from RT to 700 °C. The superior mechanical characteristics of nanocrystalline Ga_2O_3 films deposited at 500 °C are derived from the interconnected network of densely packed, nano-crystallites. The enhanced H, E_r, H/E_r, and H^3/E_r^2 values suggest that the nanocrystalline Ga_2O_3 films deposited at 500–600 °C are ideal for integration into energy related applications, where extreme or tough conditions exists. The functional relationship between microstructure and mechanical behavior of Ga_2O_3 films can serve as a road-map to produce materials for desired technological applications.

Acknowledgement

Authors acknowledge, with pleasure, support from the National Science Foundation (NSF) with grant # ECCS-1509653.

Conflict of Interest

The authors declare no conflict of interest.

Keywords

Ga_2O_3, mechanical properties, sensors, structure, thin films

Received: November 23, 2017
Revised: February 3, 2018
Published online: August 10, 2018

[1] G. Eranna, B. C. Joshi, D. P. Runthala, R. P. Gupta, *Crit. Rev. Solid State Mater. Sci*. **2004**, *29*, 111.
[2] A. E. Romanov, S. I. Stepanov, V. I. Nikolaev, V. E. Bougrov, *Rev. Adv. Mater. Sci* **2016**, *44*, 63.
[3] V. A. Shvets, V. S. Aliev, D. V. Gritsenko, S. S. Shaimeev, E. V. Fedosenko, S. V. Rykhlitski, V. V. Atuchin, V. A. Gritsenko, V. M. Tapilin, H. Wong, *J. Non. Cryst. Solids* **2008**, *354*, 3025.
[4] C. V. Ramana, R. S. Vemuri, V. V. Kaichev, V. A. Kochubey, A. A. Saraev, V. V. Atuchin, *ACS Appl. Mater. Interfaces* **2011**, *3*, 4370.
[5] H. Liu, D. Chi, *J. Vac. Sci. Technol. A Vac. Surf. Film* **2012**, *30*, 04D102.
[6] V. V. Atuchin, V. N. Kruchinin, Y. Hoong Wong, K. Y. Cheong, *Mater. Lett*. **2013**, *105*, 72.
[7] E. J. Rubio, V. V. Atuchin, V. N. Kruchinin, L. D. Pokrovsky, I. P. Prosvirin, C. V. Ramana, *J. Phys. Chem. C* **2014**, *118*, 13644.
[8] V. N. Kruchinin, T. V. Perevalov, V. V. Atuchin, V. A. Gritsenko, A. I. Komonov, I. V. Korolkov, L. D. Pokrovsky, C. W. Shih, A. Chin, *J. Electron. Mater.* **2017**, *46*, 6089.
[9] W. A. Hadi, M. S. Shur, S. K. O'Leary, *J. Mater. Sci. Mater. Electron*. **2014**, *25*, 4675.
[10] F. K. Shan, G. X. Liu, W. J. Lee, G. H. Lee, I. S. Kim, B. C. Shin, *J. Appl. Phys*. **2005**, *98*, 235041.
[11] M. Ogita, N. Saika, Y. Nakanishi, Y. Hatanaka, *Appl. Surf. Sci*. **1999**, *142*, 188.
[12] E. Fortunato, L. Raniero, L. Siva, A. Gonçalves, A. Pimentel, P. Barquinha, H. Águas, L. Pereira, G. Gonçalves, I. Ferreira, E. Elangovan, R. Martins, *Sol. Energy Mater. Sol. Cells* **2008**, *92*, 1605.
[13] G. A. Battiston, R. Gerbasi, M. Porchia, R. Bertoncello, F. Caccavale, *Thin Solid Films* **1996**, *279*, 115.
[14] S. Jin, X. Wang, X. Wang, M. Ju, S. Shen, W. Liang, Y. Zhao, Z. Feng, H. Y. Playford, R. I. Walton, C. Li, *J. Phys. Chem. C* **2015**, *119*, 18221.
[15] M. W. Knight, T. Coenen, Y. Yang, B. J. M. Brenny, M. Losurdo, A. S. Brown, H. O. Everitt, A. Polman, *ACS Nano* **2015**, *9*, 2049.
[16] M. M. Muhammed, M. A. Roldan, Y. Yamashita, S.-L. Sahonta, I. A. Ajia, K. Iizuka, A. Kuramata, C. J. Humphreys, I. S. Roqan, *Sci. Rep*. **2016**, *6*, 297471.
[17] G. O. Peapod, C. S. Nanowires, Y. Wu, C. Hsieh, P. Chen, J. Li, L. Chou, L. Chen, *ACS Nano* **2010**, *4*, 1393.
[18] N. Syed, A. Zavabeti, M. Mohiuddin, B. Zhang, Y. Wang, R. S. Datta, P. Atkin, B. J. Carey, C. Tan, J. van Embden, A. S. R. Chesman, J. Z. Ou, T. Daeneke, K. Kalantar-zadeh, *Adv. Funct. Mater.* **2017**, *27*, 1.
[19] A. Ortiz, J. C. Alonso, E. Andrade, C. Urbiola, *J. Electrochem. Soc*. **2001**, *148*, F26.
[20] M. Higashiwaki, K. Sasaki, H. Murakami, Y. Kumagai, A. Koukitu, A. Kuramata, T. Masui, S. Yamakoshi, *Semicond. Sci. Technol*. **2016**, *31*, 34001.
[21] H. J. Chun, Y. S. Choi, S. Y. Bae, H. W. Seo, S. J. Hong, J. Park, H. Yang, *J. Phys. Chem. B* **2003**, *107*, 9042.
[22] C. Kranert, C. Sturm, R. Schmidt-Grund, M. Grundmann, *Sci. Rep*. **2016**, *6*, 359641.
[23] I. Lopez, A. D. Utrilla, E. Nogales, B. Mendez, J. Piqueras, A. Peche, J. Ramírez-castellanos, J. M. Gonzalez-calbet, *J. Phys. Chem. C* **2012**, *116*, 3935.
[24] S. S. Kumar, E. J. J. Rubio, M. Noor-A-Alam, G. Martinez, S. Manandhar, V. Shutthanandan, S. Thevuthasan, C. V. Ramana, *J. Phys. Chem. C* **2013**, *117*, 4194.
[25] J. Kim, T. Sekiya, N. Miyokawa, N. Watanabe, K. Kimoto, K. Ide, Y. Toda, S. Ueda, N. Ohashi, H. Hiramatsu, H. Hosono, T. Kamiya, *NPG Asia Mater.* **2017**, *9*, e3591.
[26] E. J. Rubio, C. V. Ramana, *Appl. Phys. Lett*. **2013**, *102*, 1919131.
[27] J. Hu, Q. Li, J. Zhan, &Kacute;. Y. Jiao, Z. Liu, S. P. Ringer, Y. Bando, *D. G. &Kacute;, ACS Nano* **2008**, *2*, 107.
[28] S. Krishnamoorthy, Z. Xia, S. Bajaj, M. Brenner, S. Rajan, *Appl. Phys. Express* **2017**, *10*, 511021.
[29] A. K. Battu, S. Manandhar, V. Shutthanandan, C. V. Ramana, *Chem. Phys. Lett*. **2017**, *684*, 363.
[30] A. B. Rahane, M. D. Mrinalini, S. Chakraborty, *J. Phys. Chem. A* **2012**, *116*, 10559.
[31] S. Manandhar, C. V. Ramana, *Appl. Phys. Lett*. **2017**, *110*, 619021.
[32] A. Leyland, A. Matthews, *Wear* **2000**, *246*, 1.
[33] L. Huang, J. Lu, M. Troyon, *Surf. Coatings Technol*. **2006**, *201*, 208.
[34] S. C. Tjong, H. Chen, *Mater. Sci. Eng. R Rep*. **2004**, *45*, 1.

[35] B. D. Beake, V. M. Vishnyakov, R. Valizadeh, J. S. Colligon, *J. Phys. D. Appl. Phys.* **2006**, *39*, 1392.
[36] H. Kolsky, *Proc. Phys. Soc. B* **1949**, *62*, 676.
[37] W. D. Nix, *Metall. Trans. A* **1989**, *20*, 2217.
[38] Y. Yee Lim, M. M. Chaudhri, *Philos. Mag. A* **1999**, *79*, 2979.
[39] A. Krell, *Int. J. Refract. Met. Hard Mater.* **1998**, *16*, 331.
[40] A. Zavabeti, J. Z. Ou, B. J. Carey, N. Syed, R. Orrell-Trigg, E. L. H. Mayes, C. Xu, O. Kavehei, A. P. O'Mullane, R. B. Kaner, K. Kalantar-Zadeh, T. Daeneke, *Science (80-.)*. **2017**, *358*, 332.
[41] B. J. Carey, J. Z. Ou, R. M. Clark, K. J. Berean, A. Zavabeti, A. S. R. Chesman, S. P. Russo, D. W. M. Lau, Z. Q. Xu, Q. Bao, O. Kevehei, B. C. Gibson, M. D. Dickey, R. B. Kaner, T. Daeneke, K. Kalantar-Zadeh, *Nat. Commun.* **2017**, *8*, 1.
[42] T. Y. Tsui, W. C. Oliver, G. M. Pharr, *J. Mater. Res.* **1996**, *11*, 752.
[43] W. C. Oliver, G. M. Pharr, *J. Mater. Res.* **2004**, *19*, 3.
[44] V. V. Atuchin, B. M. Ayupov, V. A. Kochubey, L. D. Pokrovsky, C. V. Ramana, Y. M. Rumiantsev, *Opt. Mater. (Amst).* **2008**, *30*, 1145.
[45] Z. Xu, J. Dai, J. Niu, N. Li, G. Huang, L. He, *J. Alloys Compd.* **2014**, *617*, 185.
[46] W. Li, D. Ming-Hui, Z. Hong-Sen, Z. Bin, *J. Alloys Compd.* **2018**, *730*, 219.
[47] C. V. Ramana, V. V. Atuchin, L. D. Pokrovsky, U. Becker, C. M. Julien, *J. Vac. Sci. Technol. A Vac. Surf. Film* **2007**, *25*, 1166.
[48] C. V. Ramana, V. H. Mudavakkat, K. K. Bharathi, V. V. Atuchin, L. D. Pokrovsky, V. N. Kruchinin, *Appl. Phys. Lett.* **2011**, *98*, 98.
[49] Y. H. Wong, V. V. Atuchin, V. N. Kruchinin, K. Y. Cheong, *Appl. Phys. A Mater. Sci. Process.* **2014**, *115*, 1069.
[50] V. M. Kalygina, I. S. Egorova, I. A. Prudaev, O. P. Tolbanov, V. V. Atuchin, *Chin. J. Phys.* **2017**, *55*, 59.
[51] J. Gong, D. J. Lipomi, J. Deng, Z. Nie, X. Chen, N. X. Randall, R. Nair, G. M. Whitesides, *Nano Lett.* **2010**, *10*, 2702.
[52] A. K. Battu, S. Manandhar, C. V. Ramana, *Adv. Mater. Interfaces* **2017**, *4*, 17003781.
[53] U. Hangen, C. L. Chen, A. Richter, *Adv. Eng. Mater.* **2015**, *17*, 1683.
[54] H. Somekawa, T. G. Nieh, K. Higashi, *Scr. Mater.* **2004**, *50*, 1361.
[55] O. M. Ivasishin, P. E. Markovsky, Y. V. Matviychuk, S. L. Semiatin, C. H. Ward, S. Fox, *J. Alloys Compd.* **2008**, *457*, 296.
[56] B. T. Kuzumaki, O. Ujiie, H. Ichinose, *Adv. Eng. Mater.* **2000**, *8575*, 416.
[57] A. Rosenkranz, L. Reinert, C. Gachot, H. Aboufadl, S. Grandthyll, K. Jacobs, F. Müller, F. Mücklich, *Adv. Eng. Mater.* **2015**, *17*, 1234.
[58] P. M. Johnson, C. M. Stafford, *ACS Appl. Mater. Interfaces* **2010**, *2*, 2108.
[59] D. Lee, M. M. Rahman, Y. Zhou, S. Ryu, *Langmuir* **2015**, *31*, 9684.
[60] J. Zhao, P. Lemoine, Z. Liu, *Diam. Relat. Mater.* **2001**, *10*, 1070.
[61] E. Pellicer, A. Varea, S. Pané, B. J. Nelson, E. Menéndez, M. Estrader, S. Suriñach, M. D. Baró, J. Nogués, J. Sort, *Adv. Funct. Mater.* **2010**, *20*, 983.
[62] J. Musil, F. Kunc, H. Zeman, H. Poláková, *Surf. Coat. Technol.* **2002**, *154*, 304.
[63] A. Lasalmonie, J. Strudel, *J. Mater. Sci.* **1986**, *21*, 1837.
[64] A. Leyland, A. Matthews, *Surf. Coat. Technol.* **2004**, *177–178*, 317.
[65] D. Sherman, D. Brandon, *Adv. Eng. Mater.* **1999**, *1*, 161.
[66] T. F. P. A. M. Korsunsky, M. R. McGurk, S. J. Bull, *Surf. Coat. Technol.* **1998**, *99*, 171.
[67] M. J. Mayo, W. D. Nix, *Acta Metall.* **1988**, *36*, 2183.
[68] Y. Gönüllü, G. C. M. Rodríguez, B. Saruhan, M. Ürgen, *Sens. Actuators B Chem.* **2012**, *169*, 151.
[69] D. Peykov, E. Martin, R. R. Chromik, R. Gauvin, M. Trudeau, *J. Mater. Sci.* **2012**, *47*, 7189.
[70] J. Chen, L. Lu, K. Lu, *Scr. Mater.* **2006**, *54*, 1913.
[71] V. Maier, K. Durst, J. Mueller, B. Backes, H. W. Höppel, M. Göken, *J. Mater. Res.* **2011**, *26*, 1421.
[72] J. Alkorta, J. M. Martínez-Esnaola, J. G. Sevillano, *Acta Mater.* **2008**, *56*, 884.
[73] U. C. Oh, J. H. Je, *J. Appl. Phys.* **1993**, *74*, 1692.
[74] J. A. Desai, A. Kumar, *Met. Mater. Int.* **2016**, *22*, 451.
[75] H. Vehoff, D. Lemaire, K. Schüler, T. Waschkies, B. Yang, *Int. J. Mater. Res.* **2007**, *98*, 259.
[76] S. J. Bull, *Tribol. Int.* **1997**, *30*, 491.
[77] H. Sojoudi, M. R. Walsh, K. K. Gleason, G. H. McKinley, *Adv. Mater. Interfaces* **2015**, *2*, 1.
[78] S. Wirasate, F. J. Boerio, *J. Adhes.* **2005**, *81*, 509.

